The Astrophysical Journal, 867:133 (8pp), 2018 November 10 https://doi.org/10.3847/1538-4357/aae4e4

Adsorption of Organic Molecules on Onion-like Carbons: Insights on the Formation of Interstellar Hydrocarbons

Haonan Qi[1], Sylvain Picaud[2], Michel Devel[3], Enwei Liang[1], and Zhao Wang[1]
[1] Guangxi Key Laboratory for Relativistic Astrophysics, Department of Physics, Guangxi University, Nanning 530004, People's Republic of China; zw@gxu.edu.cn
[2] Institut UTINAM, CNRS UMR 6213, Université Bourgogne Franche-Comté, F-25030 Besançon, France
[3] FEMTO-ST institute, UBFC, CNRS, ENSMM, 15B avenue des Montboucons, F-25030 Besançon, France
Received 2018 June 4; revised 2018 September 21; accepted 2018 September 24; published 2018 November 7

Abstract

Using atomistic simulations, we characterize the adsorption process of organic molecules on carbon nanoparticles, both of which have been reported to be abundant in the interstellar medium (ISM). The aromatic organics are found to adsorb more readily than the aliphatic ones. This selectivity would favor the formation of polycyclic aromatic hydrocarbons (PAHs) or fullerene-like structures in the ISM due to a structural similarity. In our simulations, we also observed that the molecules form a monolayer over the nanoparticle surface before stacking up in aggregates. This suggests a possible layer-by-layer formation process of onion-like nanostructures in the ISM. These findings reveal the possible role of carbon nanoparticles as selective catalysts that could provide reaction substrates for the formation of interstellar PAHs, high fullerenes, and soots from gas-phase molecules.

Key words: astrochemistry – dust, extinction – evolution – ISM: molecules – methods: numerical – molecular data

Supporting material: tar.gz file

1. Introduction

Recent observations via the Infrared Space Observatory (ISO) and ground-based radio telescopes have pointed to the abundance of diverse carbonaceous solids in the interstellar medium (ISM; Ehrenfreund & Charnley 2000; Pirali et al. 2007). Different forms of cosmic carbon materials have been reported, including fullerenes, diamonds, graphite, soots, and so on (Kroto & Jura 1992; Henning & Salama 1998; Cami et al. 2010). These carbon solids are likely to play key roles in the physical and chemical evolution of the ISM (García-Hernández et al. 2010; Chen et al. 2017; Krasnokutski et al. 2017). Besides the carbon solids, organic molecules have also been proven to be abundant in the ISM, as evidenced by recent space and ground observations (Müller et al. 2001; Kaiser 2002; Herbst & van Dishoeck 2009; Belloche et al. 2013, 2014; Etim et al. 2016; Ceccarelli et al. 2017; Weaver et al. 2017) as well as by laboratory investigations on meteoritic samples (Henning & Salama 1998; Geppert et al. 2006; Rotelli et al. 2016). The aggregation of small organic molecules is hypothesized to provide a source for the formation of complex organic molecules, including amino acids in the primitive Earth atmosphere (Miller & Urey 1959), while the processes included in the evolution of the ISM (Jones & Nuth 2011; Chiar et al. 2013; Scoville et al. 2017) that led to the origin of life are still in a puzzle (Ehrenfreund et al. 2006; Piani et al. 2017; Puzzarini et al. 2017).

Gas-phase molecules are suspected to be elemental building blocks of complex interstellar organic molecules, many of which are polycyclic aromatic hydrocarbons (PAHs; Tielens 2008). Interstellar PAHs carry a number of broad infrared emission features, e.g., the 2175 Å UV extinction (Blasberger et al. 2017). Similarly, fullerenes of various sizes are diffuse interstellar band carriers (Iglesias-Groth 2007; Salama et al. 2011; Campbell et al. 2015; Omont 2016). The presence of PAHs and carbon nanoparticles has been invoked to explain the atmospheric composition of exoplanets, such as the warm Jupiter HD 189733b (Mousis et al. 2011). Moreover, an analysis on Allende meteorites by laser desorption mass spectrometry (LDMS) and microscopy experiments has shown onion-like nano-structures of higher fullerenes (Rotundi et al. 1998; Becker et al. 1999; Jäger et al. 2006; Krasnokutski et al. 2017). The presence of grain-layered carbon nanostructures in the ISM has therefore been unambiguously proposed in many studies (Chiar et al. 2013; Shi et al. 2015; Anderson et al. 2017). Meanwhile, very little is known about the interaction between these carbon nanostructures and the surrounding molecules (Demarais et al. 2012) and about their coupled roles in the evolution of the ISM.

Following the development of microscopic sensing devices, the adsorption of small molecules on carbon nanotubes and graphene has been intensively studied (Liu et al. 2017). An interesting feature is that usually the adsorption enthalpy increases and then decreases with increasing molecule coverage (Lazar et al. 2013). In our previous works, the interaction between water molecules and carbon soots was theoretically investigated on the grounds of astronomical and environmental interests (Moulin et al. 2007; Hantal et al. 2010; Mousis et al. 2011), and molecule aggregation was found to depend on various parameters of the adsorption environment. Molecular adsorption has also been shown to modify the optical properties of soot primary nanoparticles (Xue et al. 2009; Fan et al. 2016). However, the interaction between organic molecules and layered carbon solids remains largely unexplored. Thus, in the present work, we characterize the adsorption of organic molecules on layered carbon nanoparticles using atomistic simulations. We focus on the effect of the molecule type and density on the aggregation process around the nanoparticle and determine the corresponding adsorption energy.

2. Methods

More than 200 different molecules have been detected in the ISM. Although many oxygen-containing organics have been detected in ISM (Weaver et al. 2017), the present work

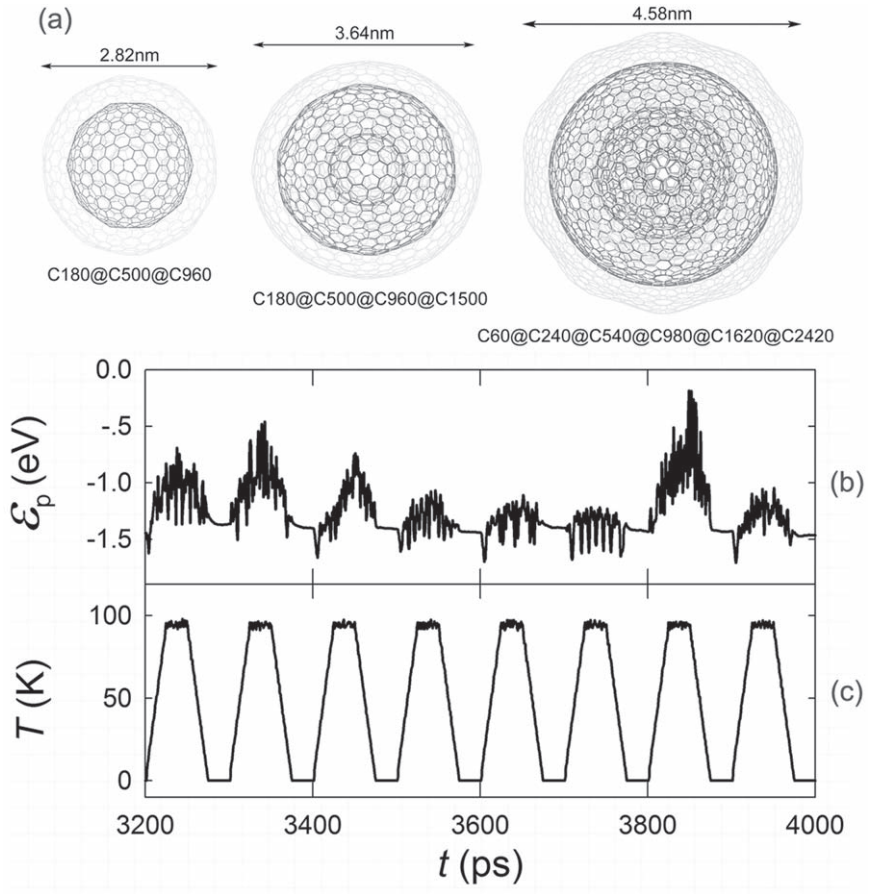

Figure 1. (a) Atomistic configurations of three "Russian doll" carbon nanoparticles studied in this work. (b)–(c) Variation of the potential energy, ε_p, and the temperature, T, of a sample during a simulation, for instance. The zero-potential value of ε_p is set to be −21767.0 eV.

focuses on carbohydrates for simplicity. Here, two aromatic (Benzene C_6H_6 and Toluene C_7H_8), two aliphatic linear (Methylpropane C_3H_8 and Hexane C_6H_{14}), and one aliphatic cyclic (Cyclopentane C_5H_{10}) organic molecule are chosen as the adsorbates in this work. The adsorption of these molecules on the carbon nanoparticles is simulated using the parallel computing package Large-scale Atomic/Molecular Massively Parallel Simulator (LAMMPS; Plimpton 1995). The carbon nanoparticles are modeled by carbon bucky-onions containing three, four, or six carbon layers (i.e., fullerenes of increasing sizes) arranged in a concentric way, as shown in Figure 1(a). The spherical fullerenes are constructed by introducing Stone-Wales defects on the edges or medians of each triangle containing a pentagon at its vertices of the icosahedral or triacontahedral fullerenes using the method introduced in Langlet et al. (2007). These generated structures of fullerenes are optimized before interacting with organics. These sp^2-hybridized carbon structures are consistent with the observations of onion-like carbons by LDMS (Becker et al. 1999) and laboratory experiments (Rotundi et al. 1998; Jäger et al. 2006). Note that the size of the nanoparticle is smaller in the simulations due to the limitation of our computational resource. The atomistic interactions between the carbon and hydrogen atoms are described in the framework of the adaptive interatomic reactive empirical bond order (AIREBO) potential (Stuart et al. 2000), in which the total interatomic potential, ε_p, involves many-body terms as a collection of those of individual bonds:

$$\varepsilon_p = \frac{1}{2}\sum_{i=1}^{N}\sum_{\substack{j=1\\ j\neq i}}^{N}\Bigg[\varphi^R(r_{i,j}) + b_{i,j}\varphi^A(r_{i,j}) + \varphi^{\mathrm{LJ}}(r_{i,j}) + \sum_{\substack{k=1\\ k\neq i,j}}^{N}\sum_{\substack{\ell=1\\ \ell\neq i,j,k}}^{N}\varphi^{\mathrm{tor}}_{kij\ell}\Bigg] \quad (1)$$

where φ^R and φ^A model the interatomic repulsion and attraction terms between the valence electrons, respectively. φ^{tor} represents the effect of single-bond torsion. The many-body effect is included in the bond order function,

$$b_{ij} = \frac{1}{2}(b_{ij}^{\sigma-\pi} + b_{ji}^{\sigma-\pi} + b_{ji}^{\mathrm{RC}} + b_{ji}^{\mathrm{DH}}) \quad (2)$$

where $b_{ij}^{\sigma-\pi}$ depends on the atomic distance and the bond angle, b_{ji}^{RC} represents the bond conjugation effect, and b_{ji}^{DH} is a dihedral-angle term for double bonds. The parameterization of this potential is provided elsewhere (Stuart et al. 2000). The long-range interactions are included by adding φ^{LJ}, a parameterized Lennard-Jones (LJ) potential with a cut-off radius of 1.0 nm. Note that φ^{LJ} applies to both the inter- and intra-molecule atomistic pairwise interactions in order to enable a smooth transition between the long-range and covalent

interactions. When compared to other force fields for hydrocarbon systems, the modeling of the bond rotation and torsion of the AIREBO potential with respect to the bond order is particularly important for simulating the adsorption process, taking into account possible deformation of the substrate induced by the adsorbate and vice versa. The AIREBO potential has therefore recently shown good accuracy in describing adsorption behaviors of systems containing sp^2- and sp^3-hybridized carbons (Petucci et al. 2013; Sun & Bai 2017).

The molecules could be adsorbed at random sites on the nanoparticle surface in a real molecular cloud. In such a process, low-energy states would finally dominate the statistics. It is thus crucial to find the possible low-energy ground states of the adsorption system. To this end, we artificially raise the temperature to transit to other metastable states. The organic molecules are initially placed at random sites on the surface of the carbon nanoparticles. The equilibrium configuration of adsorption is computed by minimizing the total potential energy, ε_p, of the system (Wang & Devel 2007; Wang et al. 2007; Wang 2009; Wang & Philippe 2009). A set of molecular dynamics (MD; Wang & Devel 2011; Lin et al. 2014; Guo et al. 2015) are then performed in order to let molecules move randomly on the surface by including a repeated annealing process, during which the temperature of the system T is controlled to switch between ~0 and 100 K, and the potential energy, ε_p, therefore circles with the variation in T, as illustrated in Figures 1(b)–(c). The temperature fluctuation here does not have realistic astrophysical sense, since the timescale in the MD simulations is not comparable to that involved in the ISM evolution. Note that there is still a probability of molecule redistribution enabled by local temperature fluctuation, since the lifetime of the interstellar molecular cloud is at the order of a million years (Elmegreen 2007).

The equations of motion are integrated by the Verlet algorithm with a time step of 0.5 fs. Below 100 K, the dynamics could be possibly dominated by ground-state motion that cannot be accurately reproduced with classical simulations. However, MD are used to perturb the system by adding thermal fluctuation before new ground-state configurations of adsorption can be generated by subsequent structural optimization. Given that the temperature of the ISM could be as low as a few Kelvins (Lippok et al. 2016), the adsorption energy, $\varepsilon_{\rm mol}$, corresponding to a ground-state (~0 K) configuration is defined as

$$\varepsilon_{\rm mol} = \frac{\varepsilon_{\rm p} - \varepsilon_{\rm np} - \varepsilon_{\rm ads}}{N}, \quad (3)$$

where $\varepsilon_{\rm np}$ stands for the potential of the nanoparticle when the small molecules are instantly removed from the surface, $\varepsilon_{\rm ads}$ is that of all organic molecules together without the nanoparticle, and N is the total number of the molecules. By this definition, $\varepsilon_{\rm mol}$ stands for the energy of the long-range (van der Waals) interaction between the nanoparticle and molecules, since the chemisorption is not considered in the present work due to the fact that only ground states are taken into account without an initially nonsaturated bond. For statistical relevance, this energy is averaged over 20 different ground-state configurations for each simulation. The number 20 has been chosen according to the results of a numerical test on the saturating potential energy with an increasing number of the samples.

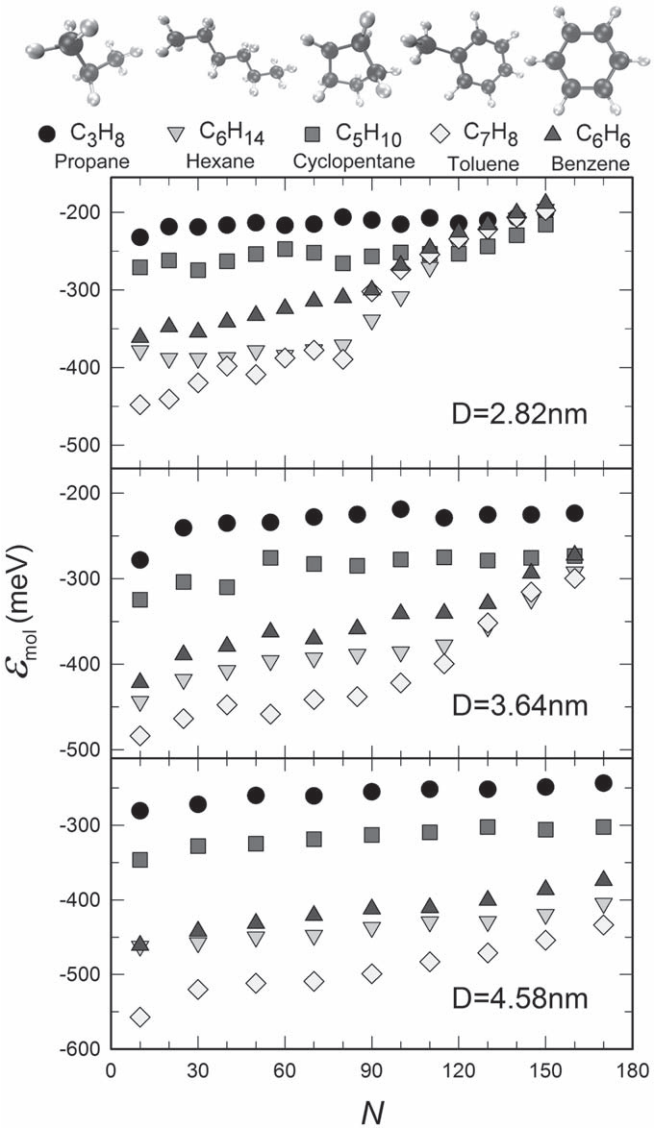

Figure 2. Adsorption energy per molecule vs. the number, N, of five different organic molecules adsorbed on three nanoparticles of different sizes.

3. Results and Discussions

Figure 2 shows the adsorption energy per molecule, $\varepsilon_{\rm mol}$, as a function of the number of adsorbed molecules, N, for the five types of organic molecules on the three carbon nanoparticles of different sizes that are considered here. $\varepsilon_{\rm mol}$ is shown to first increase with increasing N before saturating at a certain value, and then increases again with N. This behavior is more significant for the relatively large molecules, C_6H_{14} and C_7H_8, than for the smaller ones and is due to a surface-coverage effect, which will be discussed below. The comparison between $\varepsilon_{\rm mol}$ for different adsorbed molecules shows that the absolute values of $\varepsilon_{\rm mol}$ are larger for the molecules with more carbon atoms, while the effect of hydrogen seems to be less significant. For instance, the toluene (C_7H_8), which has the largest number of carbon atoms, is most strongly adsorbed to the surface among the species investigated here, while $|\varepsilon_{\rm mol}|$ for the hexanes (C_6H_{14}) is found to be slightly higher than that for the benzenes (C_6H_6). This is because the interactions are dominated by van der Waals interactions, while the LJ potential

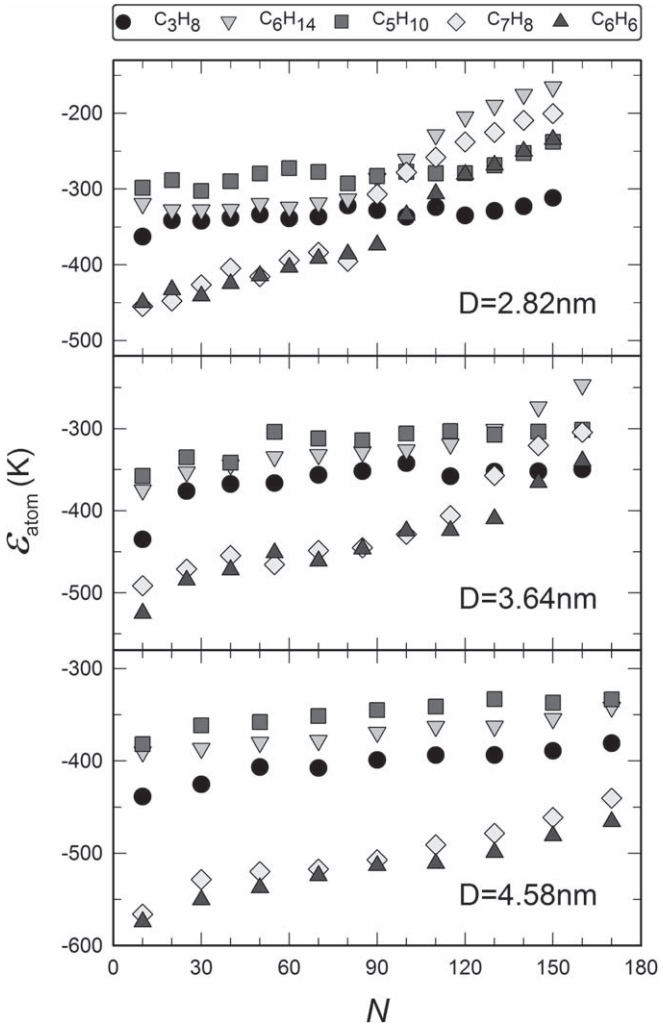

Figure 3. Adsorption energy per atom (in Kelvin) vs. the number, N, of organic molecules for the five molecule types on three nanoparticles of different sizes.

well for C–H is only 0.5523 of that for a C–C interaction (Stuart et al. 2000). Note that the results of an alternative definition of the adsorption energy are provided in Appendix A.

$\varepsilon_{\rm mol}$ includes the effects of both the atom number and the molecule geometry. To discriminate more clearly between these two effects, we define an adsorption energy per atom as

$$\varepsilon_{\rm atom} = \frac{\varepsilon_{\rm mol}}{n_C + \xi n_H}, \quad (4)$$

where n_C and n_H are the numbers of carbon and hydrogen atoms in the molecule, respectively. The parameter, ξ, is taken to be 0.5523, the ratio between the C–H and C–C equilibrium interaction potentials given in the parameters for the LJ function (Stuart et al. 2000).

In Figure 3, we plot $\varepsilon_{\rm atom}$ as a function of N to highlight the effect of the molecule shape on the adsorption energy. The aromatic molecules C_6H_6 and C_7H_8 can be seen to exhibit high absolute values of the adsorption energy, while that of the linear molecules C_3H_8 and C_6H_{14} are characterized to be lower. The cyclopentane (C_5H_{10}) is found to have the lowest absolute values of adsorption energy. As the number of the molecules increases beyond a certain threshold, the slope of the energy

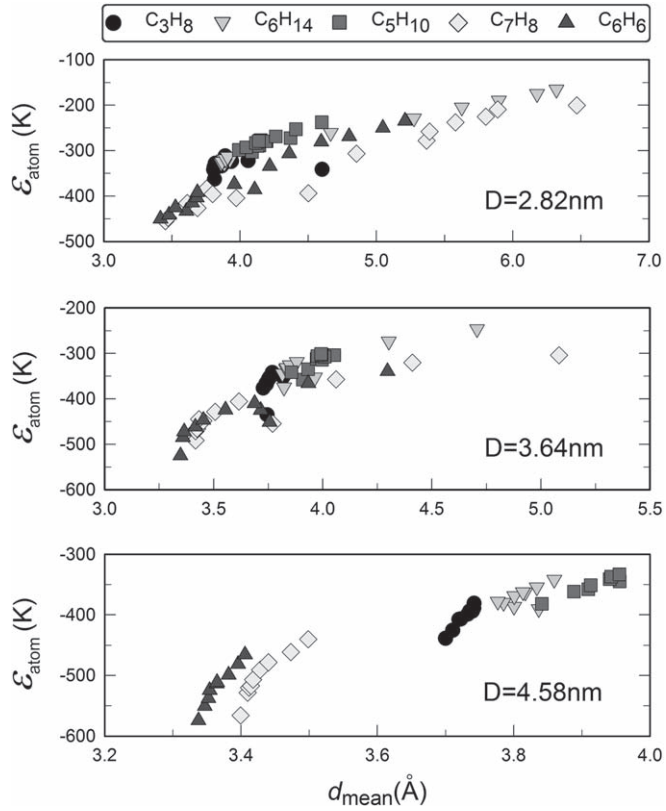

Figure 4. Adsorption energy per atom vs. mean atomistic adsorbate–substrate spacing for various molecule numbers on three nanoparticles of different sizes.

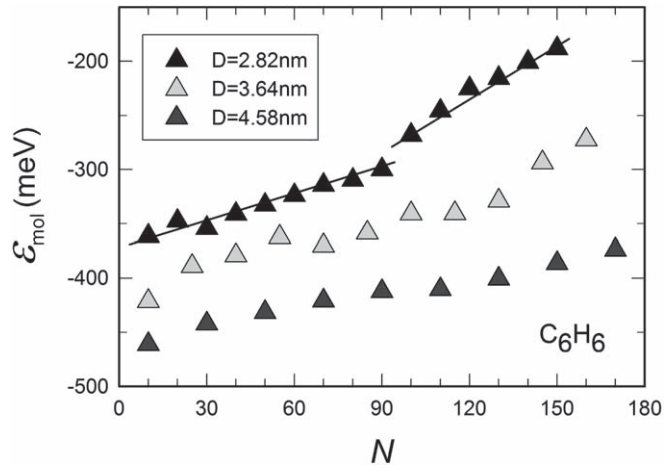

Figure 5. Adsorption energy per molecule as a function of the number, N, of C_6H_6 adsorbed on three nanoparticles of different sizes.

curve changes due to aggregation of the molecules, as we are going to discuss below. Since the energy is calculated for physisorption in this work, the energy magnitudes are generally smaller than those for chemical adsorption (Hama & Watanabe 2013; Wakelam et al. 2017; Das et al. 2018).

The values of the adsorption energy are found to be strongly correlated to the average interatomic spacing, $d_{\rm mean}$, between the molecules and nanoparticle surface, as shown in Figure 4. We can see that the per-atom adsorption energy increases with increasing mean atomistic adsorbate–substrate spacing in a power-law manner, as determined by the LJ interaction potential function. The values of the atomistic

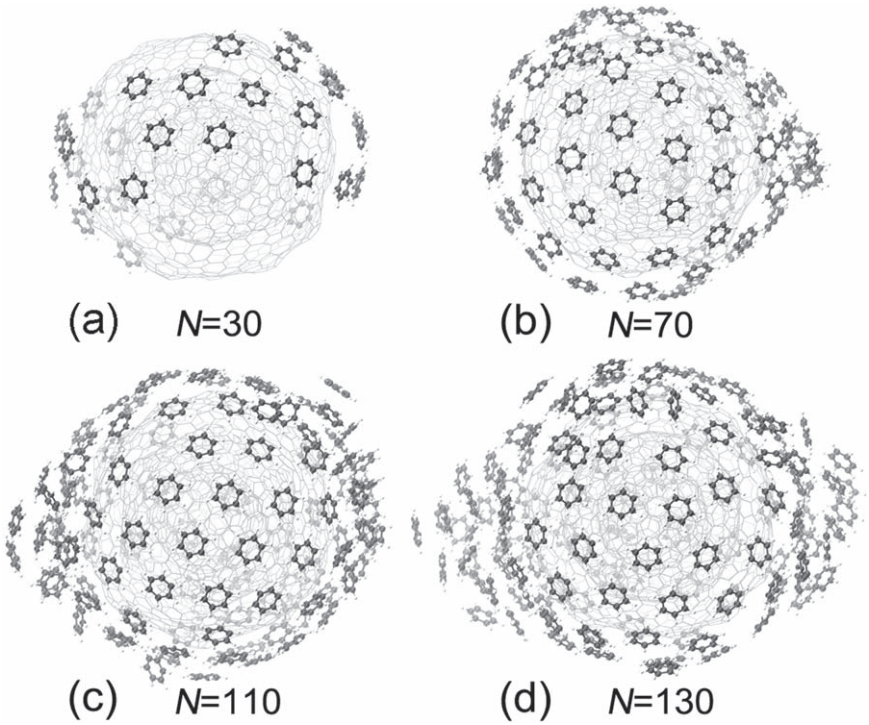

Figure 6. Atomistic configurations of the adsorbed benzene molecules on a carbon nanoparticle $D = 2.82$ nm with different surface coverages with (a) $N = 30$, (b) $N = 70$, (c) $N = 110$, (d) $N = 130$. The carbon and hydrogen atoms in benzenes are represented by black and white spheres, respectively.

adsorbate–substrate spacing are also plotted in Appendix B as functions of the number, N. The differences in the values of $d_{\rm mean}$ could be related to the contact commensurability between the lattices of the adsorbate and substrate (Verhoeven et al. 2004), which seems to favor the adsorption of aromatic (hexagonal) molecules by a preferred way of π–π stacking. We also note that the values of $d_{\rm mean}$ calculated for the hexane (C_6H_{14}) first decrease when N starts to increase. This trend is due to the bending of the carbon chain, as shown by the inset of Figure 9, which thus appears to be as a particular adsorption feature of the linear molecules. This feature highlights the influence of the structural flexibility on the adsorption of chain-shaped molecules.

The reaction process for the formation of the PAHs from organic molecules is an open question. Benzene molecules are suspected to be the building blocks of PAHs in the ISM (Joblin & Cernicharo 2018). To reveal the role of the carbon solid in such a transformation, we plot the adsorption energy of benzene molecules on three nanoparticles of different sizes in Figure 5. The adsorption energy per molecule, $\varepsilon_{\rm mol}$, can be seen to decrease as the nanoparticle size increases. This is expected since a larger nanoparticle will have a flatter surface, which is supposed to favor the adsorption. More importantly, the different slopes of the eye-guide lines in Figure 5 show that the molecules interact stronger with the nanoparticle than with other molecules. This implies that the energy-optimized stacking manner of the molecules exhibits a 2D manner, i.e., on the nanoparticle surface, it is energetically favorable that molecules form a thin layer instead of stacking up in a 3D aggregate. This is double-confirmed by computing the potential energy of molecule–molecule interactions, as shown by the table in Appendix C. The energy magnitude of the molecule–molecule interaction is smaller than that of the molecules–nanoparticle interaction shown in Figure 2. Moreover, the behavior of the adsorption energy is seen to be strongly correlated with the surface coverage, in particular, for the smallest nanoparticle with $D = 2.82$ nm.

Indeed, when a small number of molecules are adsorbed, they are observed to distribute homogeneously on the nanoparticle surface, forming a thin monolayer, as shown in Figures 6(a) and (b). The absolute value of the adsorption energy is roughly a linear function of the number of adsorbed molecules, before the surface is saturated (Figure 5). After the nanoparticle surface is about to be fully covered with increasing adsorbed molecules, added molecules start to stack up to form 3D aggregates, as shown in Figures 6(c) and (d). The progressive stacking of molecules leads to another linear increase of the adsorption energy, however, with lower energy magnitude.

By considering that a benzene molecule has roughly a radius of 0.263 nm, and by taking into account the LJ parameter of the benzene–benzene interaction model, we estimate that each benzene molecule roughly covers a surface of 0.35 nm^2. Given that the calculations show that benzene molecules are adsorbed at a distance of about 0.339 nm to the particle surface, the surface area of the benzene layer directly in contact with the nanoparticle can be estimated to be equal to about 38, 58 or 87 nm^2 for the particle of a diameter of 2.82, 3.64, or 4.58 nm, respectively. This leads to a rough estimation of the maximum number of the benzene molecules that can be packed in a homogeneously saturated ad layer that is in direct contact with the nanoparticle, which equals to about 108, 165, or 248 molecules for the nanoparticle of a diameter of 2.82, 3.64, and 4.58 nm, respectively.

Thus, the maximum number of molecules considered in the present simulations (180 benzene molecules) is a priori that is not sufficiently large enough to saturate fully the first layer of the largest nanoparticle simulated here. This could explain why

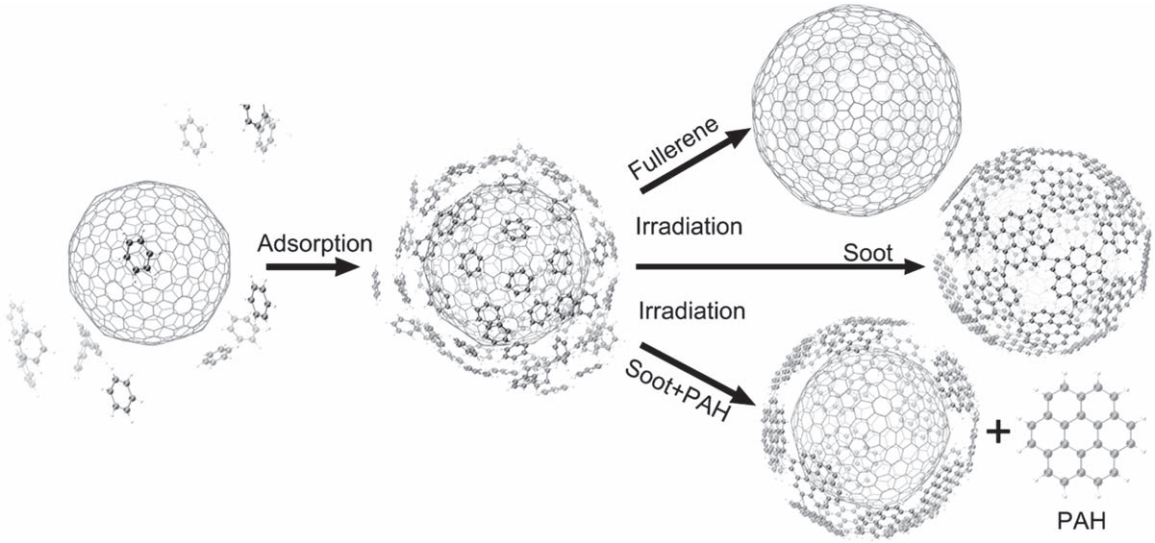

Figure 7. Schematics of a hypothesis on the formation processes of the high fullerene, soot, and PAHs from organic molecules adsorbed on a nanoparticle in the ISM.

ε_{mol} increases smoothly with N for the largest nanoparticle, without experiencing the slope break that is observed for the smallest nanoparticle. This energetic difference highlights the difference between the molecule–nanoparticle and molecule–molecule adsorptions and leads to a hypothesis about the PAH processing in interstellar molecular clouds, as suggested below. Moreover, we provide a number of atomistic configurations of the adsorbed molecules on different nanoparticles (see Appendix D), which will be useful for investigations on optical properties of carbonaceous structures in the ISM.

4. Conclusion

In conclusion, the adsorption of various organics on carbon nanoparticles of different sizes is investigated by atomistic simulations. Our results show that the aromatic molecules exhibit stronger interactions with the nanoparticles than the aliphatic ones. Thus, in the presence of possible external stimulation and consequential thermal fluctuation in the ISM environment, this selectivity may favor the formation of sp^2-hybridized carbon nanostructures, such as PAHs or fullerene-like layers due to a similarity in their atomic structure and bond conjugation. Note that the temperature variation technique employed in the simulations is unrelated to the aforementioned thermal fluctuation in the ISM. As observed in our simulations, the molecules spontaneously form a homogeneous layer over the nanoparticle surface before stacking up in 3D aggregations. This indicates a possible layer-by-layer formation process of onion-like nanostructures in the ISM. This is also based on the fact that the interaction energy is lower in absolute values between molecules in aggregations than between molecules and nanoparticles. Since the timescale for in the ISM evolution is so long (Elmegreen 2007), redistribution of molecules over the nanoparticle surface could be enabled by external stimulation or by local temperature fluctuation, and low-energy states would finally dominate the statistics. Hence, with the energy input from the expected stimulation processes into the nanoparticle or molecules, the energy difference between molecule–molecule and molecule–nanoparticle interactions can lead to selectively disperse aggregations, while keeping a homogeneous layer over the nanoparticle surface.

The above results demonstrated a physisorption process in the ISM as the first step of chemisorption and lead to the hypotheses illustrated in Figure 7 on the formation of layered carbon nanoparticles and PAHs from elementary molecules in the ISM. In such a scheme, gas-phase molecules, preferably aromatic, are adsorbed on the surface of small nanoparticles, as evidenced in the present theoretical study. Irradiation (by cosmic-ray particles, UV photons, etc. (Zheng et al. 2008; Chiar et al. 2013)) would lead to the formation of various possible nanostructures depending on the magnitude of dehydrogenation: e.g., onion-like fullerenes, PAHs or soots (a priori PAH clusters). We should note that the hypotheses illustrated in Figure 7 are idealized. In real ISM environment, the accretion of other abundant gaseous species including aliphatic molecules would inhibit the successive assembly of aromatic molecules, despite aromatic molecules are adsorbed stronger than other ones. Thus, the surface density of aromatic and aliphatic molecules should depend on their gas-phase abundances. These findings have implications on the formation of layered carbon nanoparticles and PAHs in the ISM (mostly in the environment of diffuse clouds) from elementary gas-phase molecules. In this scenario, the possible catalyst role of the nanoparticles is hypothesized for the molecular complexity in the ISM, as an initial aspect in the nucleation and growth of interstellar dust, and in the formation of stars and planets.

Jesús Carrete is acknowledged for proofreading of this manuscript. This work has been supported by the Guangxi Science Foundation (2018GXNSFAA138179, 2013GXNSFFA019001), Scientific Research Foundation of Guangxi University (XTZ160532), Guangxi Key Laboratory Foundation (15-140-54), National Natural Science Foundation of China (11533003 and U1731239), EIPHI Graduate School (ANR-17-EURE-0002), and Region Bourgogne Franche-Comté.

Appendix A
An Alternative Adsorption Energy

Alternatively, the adsorption energy can be defined as the amount of energy needed to bring together the nanoparticle and

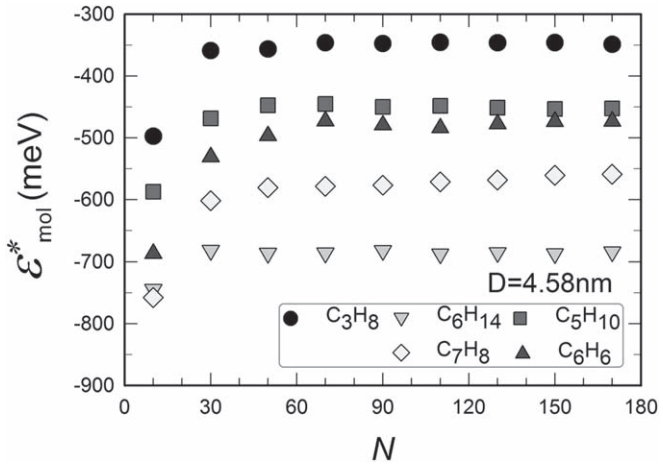

Figure 8. Adsorption energy per molecule vs. the number, N, of organic molecules adsorbed on a nanoparticle that is 4.58 nm in diameter.

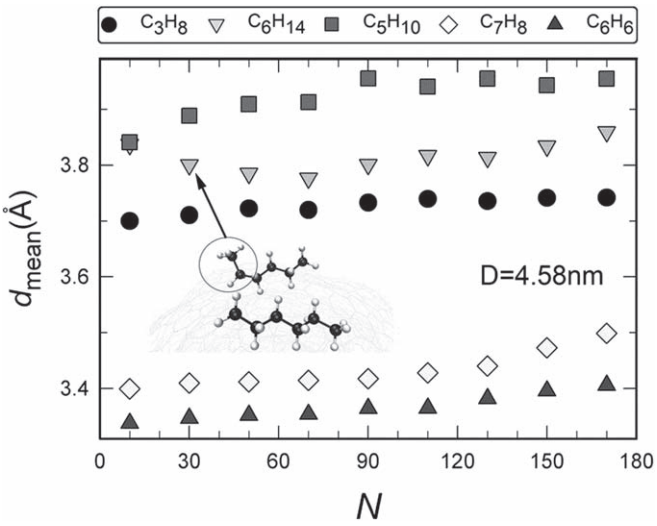

Figure 9. Mean atomistic adsorbate–substrate spacing as functions of the number, N, of organic molecules for the nanoparticle $D = 4.58$ nm.

Table 1
Molecule–Molecule Interaction Energy Values

ε_{mol} (meV)	C_6H_6	C_5H_{10}	C_6H_{14}	C_3H_8	C_7H_8
ε_{min}	−17.02	−63.91	−33.34	−36.89	−27.06
ε_{max}	−154.06	−12.171	−166.58	−80.17	−212.21
ε_{ave}	−81.71	−90.22	−116.46	−61.48	−158.67

molecules from infinite-far:

$$\varepsilon^* = \varepsilon_{total} - \varepsilon^*_{np} - N\varepsilon^*_{ads}, \quad (5)$$

where ε^*_{np} is the minimized potential energy of the nanoparticle, and ε^*_{ads} is that of a single adsorbate. Figure 8 shows the adsorption energy per molecule by this definition as a function of the number of organic molecules.

Appendix B
Atomistic Adsorbate–Substrate Spacing

Figure 9 shows the mean atomistic adsorbate–substrate spacing as functions of the number, N, of organic molecules.

Appendix C
Molecule–Molecule Interaction Energy

Table 1 gives the molecule–molecule interaction energy that has been calculated using 12 different equilibrium configurations of two molecules together. ε_{min} and ε_{max} give the minimum and maximum values in the 20 samples with various initial configurations, respectively. ε_{ave} gives the mean.

Appendix D
Atomistic Coordinate Data Files

Data files that contain optimized atomistic configurations of organic molecules adsorbed on onion-like nanoparticles are provided online in the supporting material. These .xyz files contain the atomistic coordinates of the adsorbed organic molecules and nanoparticles by giving the total number of atoms that will be read on the first line; the numbers of molecules, atoms in each molecule, and atoms in the nanoparticle on the second; and the atom type and three atomic Cartesian coordinates in the following lines. Please see the PDF in the zipped Enhanced Manuscript Information file for a complete list and instructions.

ORCID iDs

Zhao Wang https://orcid.org/0000-0003-1887-223X

References

Anderson, D. E., Bergin, E. A., Blake, G. A., et al. 2017, ApJ, 845, 13
Becker, L., Bunch, T. E., & Allamandola, L. J. 1999, Natur, 400, 227
Belloche, A., Garrod, R. T., Müeller, H. S. P., & Menten, K. M. 2014, Sci, 345, 1584
Belloche, A., Müeller, H. S. P., Menten, K. M., Schilke, P., & Comito, C. 2013, A&A, 559, A47
Blasberger, A., Behar, E., Perets, H. B., Brosch, N., & Tielens, A. G. G. M. 2017, ApJ, 836, 173
Cami, J., Bernard-Salas, J., Peeters, E., & Malek, S. E. 2010, Sci, 329, 1180
Campbell, E. K., Holz, M., Gerlich, D., & Maier, J. P. 2015, Natur, 523, 322
Ceccarelli, C., Caselli, P., Fontani, F., et al. 2017, ApJ, 850, 176
Chen, X. H., Li, A., & Zhang, K. 2017, ApJ, 850, 104
Chiar, J. E., Tielens, A. G. G. M., Adamson, A. J., & Ricca, A. 2013, ApJ, 770, 78
Das, A., Sil, M., Gorai, P., Chakrabarti, S. K., & Loison, J. C. 2018, ApJS, 237, 9
Demarais, N. J., Yang, Z., Martinez, O., Jr., et al. 2012, ApJ, 746, 32
Ehrenfreund, P., & Charnley, S. B. 2000, ARA&A, 38, 427
Ehrenfreund, P., Rasmussen, S., Cleaves, J., & Chen, L. 2006, AsBio, 6, 490
Elmegreen, B. G. 2007, ApJ, 668, 1064
Etim, E. E., Gorai, P., Das, A., Chakrabarti, S. K., & Arunan, E. 2016, ApJ, 832, 144
Fan, M., Chen, L., Li, S., et al. 2016, Aerosol Air Quality Res., 16, 1315
García-Hernández, D. A., Manchado, A., García-Lario, P., et al. 2010, ApJL, 724, L39
Geppert, W. D., Hamberg, M., Thomas, R. D., et al. 2006, FaDi, 133, 177
Guo, W., Wang, Z., & Li, J. 2015, NanoL, 15, 6582
Hama, T., & Watanabe, N. 2013, ChRv, 113, 8783
Hantal, G., Picaud, S., Hoang, P. N. M., et al. 2010, JChPh, 133, 144702
Henning, T., & Salama, F. 1998, Sci, 282, 2204
Herbst, E., & van Dishoeck, E. F. 2009, ARA&A, 47, 427
Iglesias-Groth, S. 2007, ApJL, 661, L167
Jäger, C., Krasnokutski, S., Staicu, A., et al. 2006, ApJS, 166, 557
Joblin, C., & Cernicharo, J. 2018, Sci, 359, 156
Jones, A. P., & Nuth, J. A. 2011, A&A, 530, A44
Kaiser, R. I. 2002, ChRv, 102, 1309
Krasnokutski, S. A., Goulart, M., Gordon, E. B., et al. 2017, ApJ, 847, 89
Kroto, H. W., & Jura, M. 1992, A&A, 263, 275
Langlet, R., Mayer, A., Geuquet, N., et al. 2007, DRM, 16, 2145
Lazar, P., Karlický, F., Jurečka, P., et al. 2013, JAChS, 135, 6372

Lin, J., Li, X., Qiao, G., et al. 2014, JAChS, 136, 1497
Lippok, N., Launhardt, R., Henning, T., et al. 2016, A&A, 592, A61
Liu, L., Tan, S. J., Horikawa, T., et al. 2017, AdCIS, 250, 64
Miller, S. L., & Urey, H. C. 1959, Sci, 130, 245
Moulin, F., Picaud, S., Hoang, P. N. M., & Jedlovszky, P. 2007, JChPh, 127, 164719
Mousis, O., Lunine, J. I., Petit, J. M., et al. 2011, ApJ, 727, 77
Müller, H. S. P., Thorwirth, S., Roth, D. A., & Winnewisser, G. 2001, A&A, 370, L49
Omont, A. 2016, A&A, 590, A52
Petucci, J., LeBlond, C., Karimi, M., & Vidali, G. 2013, JChPh, 139, 044706
Piani, L., Tachibana, S., Hama, T., et al. 2017, ApJ, 837, 35
Pirali, O., Vervloet, M., Dahl, J. E., et al. 2007, ApJ, 661, 919
Plimpton, S. 1995, JCoPh, 117, 1
Puzzarini, C., Baiardi, A., Bloino, J., et al. 2017, ApJ, 154, 82
Rotelli, L., Trigo-Rodríguez, J. M., Moyano-Cambero, C. E., et al. 2016, NatSR, 6, 38888
Rotundi, A., Rietmeijer, F. J. M., Colangeli, L., et al. 1998, A&A, 329, 1087
Salama, F., Galazutdinov, G. A., Krelowski, J., et al. 2011, ApJ, 728, 154
Scoville, N., Lee, N., Bout, P. V., et al. 2017, ApJ, 837, 150
Shi, J., Grieves, G. A., & Orlando, T. M. 2015, ApJ, 804, 24
Stuart, S. J., Tutein, A. B., & Harrison, J. A. 2000, JChPh, 112, 6472
Sun, C., & Bai, B. 2017, PCCP, 19, 3894
Tielens, A. G. G. M. 2008, ARA&A, 46, 289
Verhoeven, G. S., Dienwiebel, M., & Frenken, J. W. M. 2004, PhRvB, 70, 165418
Wakelam, V., Loison, J. C., Mereau, R., & Ruaud, M. 2017, MolAs, 6, 22
Wang, Z. 2009, Carbon, 47, 3050
Wang, Z., & Devel, M. 2007, PhRvB, 76, 195434
Wang, Z., & Devel, M. 2011, PhRvB, 83, 125422
Wang, Z., Devel, M., Langlet, R., & Dulmet, B. 2007, PhRvB, 75, 205414
Wang, Z., & Philippe, L. 2009, PhRvL, 102, 215501
Weaver, S. L. W., Laas, J. C., Zou, L., et al. 2017, ApJS, 232, 3
Xue, H., Khalizov, A. F., Wang, L., Zheng, J., & Zhang, R. 2009, PCCP, 11, 7869
Zheng, W., Jewitt, D., Osamura, Y., & Kaiser, R. I. 2008, ApJ, 674, 1242